Article:
Ding, J., Della Santina, C., Lam, T.L. et al. (4 more authors) (2024) Robust Humanoid Locomotion via Sequential Stepping and Angular Momentum Optimization. IEEE Transactions on Industrial Electronics. ISSN 0278-0046

https://doi.org/10.1109/TIE.2024.3433451

Robust Humanoid Locomotion via Sequential Stepping and Angular Momentum Optimization

Jiatao Ding, Cosimo Della Santina, Tin Lun Lam*, Jianxin Pang*,
Xiaohui Xiao, Nikos Tsagarakis, and Yanlong Huang

***Abstract*—Stepping strategy, including step time and step location modulation, and hip strategy, i.e., upper-body movement, play crucial roles in achieving robust humanoid locomotion. However, exploiting these balance strategies in a unified and flexible manner has not been well addressed. In this work, we propose a sequential convex optimization approach. Based on the linear inverted pendulum model, we modulate step parameters, including step location and step time, using quadratically constrained quadratic programming in real time. Then, based on the nonlinear inverted pendulum plus flywheel model, we regulate angular momentum using the linear model predictive control. To accommodate for scenarios with height variation, we consider nonlinear 3D locomotion dynamics explicitly. The proposed approach is validated via comparison studies and extensive experiments on the humanoid with planar and linear feet. The results demonstrate enhanced robustness against dynamic disturbances and adaptability to real-world scenarios. On average, the enhanced stepping strategy rejects 135% larger external forces than our previous work. Also, robust locomotion across height-varying stepping stones is realized, which is rarely reported for a humanoid robot with planar feet.**

***Index Terms*—Robust locomotion, optimization, angular momentum, step time modulation, humanoid robot.**

I. Introduction

HUMANOID locomotion is a challenging task due to high-dimensional hybrid nonlinear dynamics and inherent instability [2]–[4]. Observations from human walking reveal that multiple balance strategies, such as reactive stepping [5], body rotation [6], and height variation [7] could be used to maintain balance. The utilization of template models, such as the 3D linear inverted pendulum (LIP) model [8], the nonlinear inverted pendulum plus a flywheel (NIPF) model [9] and virtual-mass-ellipsoid inverted pendulum [10], makes it possible to obtain time-efficient solutions for robust locomotion [11], [12]. However, exploiting multiple strategies in a unified and flexible manner, which is required in achieving robust locomotion in challenging scenarios, e.g., push recovery when walking across height-varying surfaces (as illustrated in Fig. 1), still needs further studies.

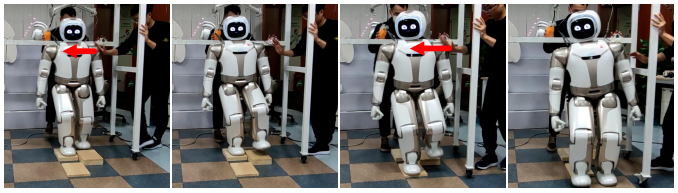

Fig. 1. The humanoid robot rejects external pushes (marked by red arrows) when walking across sparse stepping stones at different heights.

A. Related work

The stepping strategy plays a crucial role in enhancing locomotion robustness, whereby the support region is extended through adjusting step locations and time online [13]–[16]. However, the modulation of step parameters, especially the step time (i.e., step duration), usually leads to computing-intensive nonlinear programming (NLP). To overcome this, [17] used quadratic programming (QP) to adjust the step time first. Then, a time-intensive model predictive strategy (MPC) strategy was needed later to optimize the step location and center of mass (CoM) trajectory. In [18] and [1], step-duration alternative variables were introduced to simplify the formulation. Particularly, the work in [18] built a QP to solve the problem efficiently, where an accurate estimation of the capture point is required. [1] formulated a quadratically constrained QP (QCQP) to adjust the step location and step time simultaneously. Nonetheless, this work adopted sequential QP (SQP) to solve the non-convex problem without guaranteeing global convergence. Aside from optimization, [5] proposed a closed-form solution for rapidly adjusting step parameters, where, however, physical constraints are ignored.

Jiatao Ding and Cosimo Della Santina are with the Department of Cognitive Robotics, Delft University of Technology, Building 34, Mekelweg 2, 2628CD, Delft, The Netherlands (e-mails: {J.Ding-2, C.DellaSantina}@tudelft.nl). Cosimo Della Santina is also with the Institute of Robotics and Mechatronics, German Aerospace Center (DLR), 82234 Wessling, Germany (e-mail: cosimodellasantina@gmail.com). Tin Lun Lam is with the School of Science and Engineering, the Chinese University of Hong Kong, Shenzhen, and Shenzhen Institute of Artificial Intelligence and Robotics for Society, Shenzhen, China (e-mail: tllam@cuhk.edu.cn). Jianxin Pang is with Ubtech Robotics Corporation, Xili street, Nanshan District, Shenzhen, 518071, Guangdong Province, China (e-mail: walton@ubtrobot.com). Xiaohui Xiao is with the School of Power and Mechanical Engineering, Wuhan University, Wuhan, 430072, Hubei Province, China (e-mail: xhxiao@whu.edu.cn). Nikos Tsagarakis is with the Humanoids and Human Centered Mechatronics research line of Istituto Italiano Di Tecnologia (IIT), Via Morego 30, 16163, Genova, Italy (e-mail: nikos.tsagarakis@iit.it). Yanlong Huang is with School of Computing, University of Leeds, Leeds, LS29JT, UK (e-mail: y.l.huang@leeds.ac.uk).

A part of preliminary results have been presented in IEEE International Conference on Intelligent Robots and Systems [1].

Furthermore, the above works ignore angular momentum regulation (i.e., hip strategy) and height variation, limiting the applications. To tackle this issue, [19] proposed a hierarchical strategy to modulate step time and angular momentum. [12] formulated a QP to integrate ankle, stepping and hip strategies together by ignoring multiplications among decision variables. [20] and [21] proposed a hybrid formulation, i.e., QP plus a closed-form solution, for modulating step parameters and angular momentum, which, however, overlooked the feasibility constraints. A constrained MPC scheme was proposed in [11] to modulate step parameters and body rotation. Nevertheless, this work, together with other aforementioned works, did not consider the nonlinear dynamics with respect to (w.r.t) height variation. The height variation was discussed in [9], [22] and then was incorporated [10] for 3D walking with momentum regulation. Nonetheless, it is difficult, if not impossible, to obtain the global optimum using the formulation in [10]. In [23], the cascaded MPC was formulated for multiple strategies integration, guaranteeing the global convergence of each smaller optimization problem. However, the step time modulation is missing.

B. Our solution & contribution

In this work, we aim for robust locomotion via sequential convex optimization. The proposed two-layer optimization structure integrates stepping (including step location and step time modulation) and hip strategy while accounting for height variation. Due to the usage of reduced-order template models, i.e., the LIP model in the first layer and the NIPF model in the second layer, efficient solutions with global convergence are achieved to fully exploit each balance strategy, which has been validated by extensive experiments.

This article has extended [1] with substantial algorithmic and experimental contributions. The contributions are

1) we generate the optimal step parameters, including step location and step time, using semidefinite relaxation (SDR). As a result, an efficient solution with global convergence is obtained. Compared with [1], the push recovery capability is largely improved;
2) we adjust angular momentum while addressing the nonlinear dynamics caused by height variations using QP, enhancing walking robustness and adaptability;
3) we validate the approach via extensive experiments. Since multiple balance strategies are integrated in a unified and flexible manner, robots achieve robust and adaptable locomotion in challenging scenarios, such as walking across height-varying stepping stones against external pushes, which has rarely been reported by humanoids with planar feet. Furthermore, the proposed approach can directly apply to the humanoid with line feet.

The rest is organized as follows: Section II provides a first glance at the proposed method. Section III and Section IV separately detail step parameters optimization and angular momentum modulation. In Section V, we validate the proposed approach by extensive tests and comparison studies. Section VI concludes this work.

II. Overview

This work aims to exploit multiple balance strategies, especially the step and hip strategies, to enhance locomotion robustness. Fig. 2 illustrates the control architecture.

As a key design choice, sequential convex optimization is proposed to generate the reactive gaits, making it possible to integrate stepping and hip strategies without bringing in a heavy computing burden. Based on the 3D LIP model, a QCQP problem is formulated first to modulate step location and step time (namely, step duration) in a real-time fashion. By virtue of SDR, the step parameters are updated at 40 Hz. Then, angular momentum is regulated by rotating the upper body. Defining the height trajectory in advance, a linear MPC (LMPC) is built to manipulate the centroidal moment pivot (CMP) [24], on the basis of the 3D NIPF model [9]. The second-layer optimization runs at 100 Hz. As a result, the stepping and hip strategies with height variation are integrated.

After modulating the gait parameters, we adopt an imitation learning scheme to generate the swing leg trajectories, providing another adaptation feature [25]. To save the space, we omit the details here.

After achieving reference motion, the admittance control scheme similar to [26] is used for tracking control. Feasibility constraints such as joint limits and friction restrictions are considered when computing joint angle commands. In real tests, a high-order sliding mode observer is used to estimate 3D CoM status and body rotation status [23]. The low-level tracking control and state estimation run at 1 KHz.

Notations: In the following sections, vectors and matrices are bold. Given a variable, $(\cdot)^2$ denotes the square operation, $\cosh(\cdot)$ and $\sinh(\cdot)$ separately denote the hyperbolic cosine and sine function, $(\cdot)^r$ and $(\cdot)^e$ separately denote the reference and estimated value, $(\cdot)^{\min}$ and $(\cdot)^{\max}$ separately denote the minimal and maximal boundary value. Other important notations are listed in Table I.

III. Reactive step via QCQP

This section details the stepping strategy. To start, we derive an analytic solution for 3D LIP. Then, we present the optimization formulation and solution.

A. 3D LIP dynamics: an analytic solution

In this stage, the 3D LIP model is employed to capture the locomotion dynamics by which the body movement, e.g., the pelvis center in the humanoid robot, is characterized by CoM motion. When walking without vertical accelerations[1], the CoP dynamics within each step cycle is determined by [8]

$$p_\gamma = c_\gamma - \ddot{c}_\gamma/(\omega_0)^2, \quad \text{with } \omega_0 = \sqrt{g/Z_c}, \tag{1}$$

where Z_c is the nominal height of the 3D LIP.

Assuming that there is no CoP movement during each step cycle, i.e., CoP coincides with the support center (as illustrated in Fig. 3(b)), Eq. (1) can be simplified as

$$\ddot{c}_\gamma = c_\gamma(\omega_0)^2. \tag{2}$$

[1] In 3D LIP, linear variation of vertical height (see the dashed red line in Fig. 3(a)) is allowed for a 3D locomotion task.

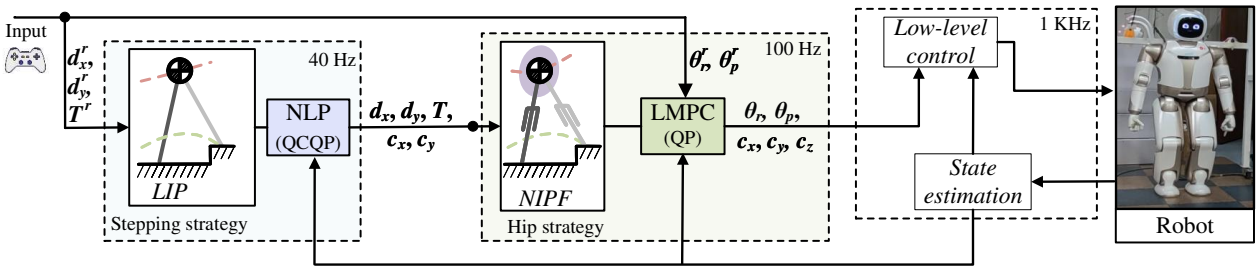

Fig. 2. Block diagram of the proposed method. The robot locomotion is obtained by sequential convex optimization that accounts for step parameters modulation and angular momentum variation. $[d_x^r, d_y^r, T^r]^\mathsf{T}$ and $[d_x, d_y, T]^\mathsf{T}$ separately denote the reference and optimized sagittal step location, lateral step location and step cycle. $[\theta_r^r, \theta_p^r]^\mathsf{T}$ and $[\theta_r, \theta_p]^\mathsf{T}$ separately denote the reference and optimized roll angle and pitch angle. $[c_x, c_y, c_z]^\mathsf{T}$ denote the optimized 3D CoM trajectory.

TABLE I
VARIABLE NOTATIONS

1. Key variables first appear in the first-layer optimization	
p_γ	Horizontal CoP position along γ- axis ($\gamma \in \{x, y\}$)
$c_\gamma, \dot{c}_\gamma, \ddot{c}_\gamma$	Horizontal CoM position, velocity and acceleration
ω_0	Constant natural frequency of the 3D LIP
$c_{\gamma(t)}, \dot{c}_{\gamma(t)}, \ddot{c}_{\gamma(t)}$	CoM position, velocity and acceleration at time t
t_e	Elapsed time of the current step
$t_{\text{ch}}/t_{\text{sh}}$	Alternative variables w.r.t $\cosh(\cdot)$ / $\sinh(\cdot)$
${}_1f({}_1\boldsymbol{\mathcal{X}})$	Cost function w.r.t decision variables ${}_1\boldsymbol{\mathcal{X}}$
dt	Sampling time for the first-stage optimization
2. Key variables first appear in the seconde-layer optimization	
cmp_γ	CMP position along γ- axis ($\gamma \in \{x, y\}$)
p_γ^h	CoP position along γ- axis w.r.t height variation
ω	Time-varying natural frequency of the NIPF model
$c_z, \dot{c}_z, \ddot{c}_z$	Vertical CoM height, velocity and acceleration
θ_r, θ_p	Roll and pitch angle of the upper body
$\ddot{\theta}_r, \ddot{\theta}_p$	Roll and pitch angular acceleration
${}_2f({}_2\boldsymbol{\mathcal{X}})$	Cost function w.r.t decision variables ${}_2\boldsymbol{\mathcal{X}}$
${}_2dt$	Sampling time for the second-stage optimization
3. Gait and model parameters	
s_x, s_y, s_z	Step length, width and height at each step cycle
d_x, d_y, d_z	3D landing location in world coordinate
T	Step time of each step
m/g	Robot mass/gravitational acceleration
$\mathbf{I}^g, \mathbf{I}_B$	Inertial matrix in the global/body coordinate system

Given the current state, i.e., CoM position $c_{\gamma(t_e)}$ and velocity $\dot{c}_{\gamma(t_e)}$ at the elapsed time t_e, the final state is

$$\begin{bmatrix} c_{\gamma(T)} \\ \dot{c}_{\gamma(T)} \end{bmatrix} = \begin{bmatrix} c_{\gamma(t_e)} & \frac{\dot{c}_{\gamma(t_e)}}{\omega_0} \\ \dot{c}_{\gamma(t_e)} & c_{\gamma(t_e)}\omega_0 \end{bmatrix} \begin{bmatrix} \cosh(\omega_0(T-t_e)) \\ \sinh(\omega_0(T-t_e)) \end{bmatrix}. \tag{3}$$

Here, we define step-duration alternative variables as

$$t_{\text{ch}} = \cosh(\omega_0(T-t_e)), \quad t_{\text{sh}} = \sinh(\omega_0(T-t_e)). \tag{4}$$

Considering $0 \le t_e \le T$, we have $0 \le T - t_e \le T$. Therefore, t_{ch} and t_{sh} are the injective functions of t_e.

Using Eq. (4), Eq. (3) can be rewritten as

$$\begin{bmatrix} c_{\gamma(T)} \\ \dot{c}_{\gamma(T)} \end{bmatrix} = \begin{bmatrix} c_{\gamma(t_e)} & \frac{\dot{c}_{\gamma(t_e)}}{\omega_0} \\ \dot{c}_{\gamma(t_e)} & c_{\gamma(t_e)}\omega_0 \end{bmatrix} \begin{bmatrix} t_{\text{ch}} \\ t_{\text{sh}} \end{bmatrix}. \tag{5}$$

From Eq. (5), we find that the CoM movement is determined by the current CoM state and the step-duration alternative variables. By virtue of this property, we can optimize the step parameters and CoM motion based on the real state.

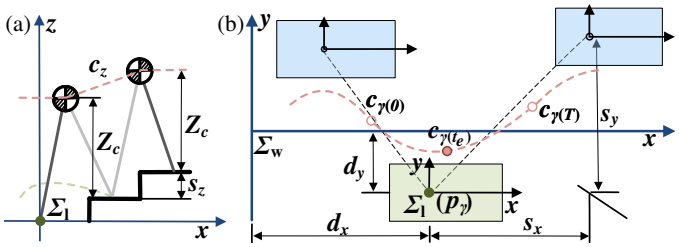

Fig. 3. 3D LIP. (a) plots the sagittal motion, and (b) plots the horizontal motion. The dashed red line in (a) plots the sagittal CoM trajectory for stair climbing, and the dashed red curve in (b) plots the horizontal CoM trajectory. The dashed green curve in (a) plots the swig leg trajectory. Σ_w and Σ_l represent the global and local origins, respectively. Green and blue blocks in (b) separately mark the right and left feet. x-, y- and z- separately point to the forward, leftward and upward direction.

B. QCQP formualtion

1) Cost function: To accomplish the desired locomotion task, we track the reference step parameters and the desired final CoM states. That is,

$${}_1f({}_1\boldsymbol{\mathcal{X}}) = \sum_{{}_1\boldsymbol{X}} \frac{\sigma_{{}_1\boldsymbol{X}}}{2} \parallel {}_1\boldsymbol{X} - {}_1\boldsymbol{X}^r \parallel^2, \tag{6}$$

where ${}_1\boldsymbol{\mathcal{X}} = [s_x, s_y, t_{\text{ch}}, t_{\text{sh}}]^\mathsf{T} \in \mathbb{R}^4$ comprises the decision variables, ${}_1\boldsymbol{X} = [{}_1\boldsymbol{\mathcal{X}}^\mathsf{T}, c_{x(T)}, c_{y(T)}, \dot{c}_{x(T)}, \dot{c}_{y(T)}]^\mathsf{T} \in \mathbb{R}^8$ comprises the variables contributing to the cost terms. $\sigma_{{}_1\boldsymbol{X}}$ denotes the weight coefficient. ${}_1\boldsymbol{X}^r \in \mathbb{R}^8$ are the corresponding reference values. For example, the $c_{x(T)}^r$, $c_{y(T)}^r$, t_{ch}^r and t_{sh}^r are determined by

$$\begin{aligned} c_{x(T)}^r &= s_x^r/2, & c_{y(T)}^r &= s_y^r/2, \\ t_{\text{ch}}^r &= \cosh(\omega_0(T^r - t_e)), & t_{\text{sh}}^r &= \sinh(\omega_0(T^r - t_e)), \end{aligned} \tag{7}$$

where T^r, s_x^r, and s_y^r are the reference step parameters.

Here, we set the reference final CoM position to be $s_\gamma/2$ to ensure that the final CoM stays in the middle of consecutive step locations. The desired CoM final velocity ($\dot{c}_{\gamma(T)}^r$) can be computed by (3) given the reference final CoM position ($c_{\gamma(T)}^r$) and the current CoM position ($c_{\gamma(t_e)}$). It is worth mentioning that, for the closed-loop control, we use the estimated CoM position ($c_{\gamma(t_e)}^e$) as the current CoM position.

2) Feasibility constraints: To obtain feasible gaits, constraints arising from the physical limitations are considered.

$$\cosh(\omega_0(\delta T^{\min})) \le t_{\text{ch}} \le \cosh(\omega_0(\delta T^{\max})), \tag{8a}$$
$$\sinh(\omega_0(\delta T^{\min})) \le t_{\text{sh}} \le \sinh(\omega_0(\delta T^{\max})), \tag{8b}$$
$$t_{\text{ch}}^2 - t_{\text{sh}}^2 = 1, \tag{8c}$$
$$s_\gamma^{\min} \le s_{\gamma(k)} \le s_\gamma^{\max}, \tag{8d}$$
$$\dot{s}_\gamma^{\min} \le (s_{\gamma(k)} - s_{\gamma(k-1)})/dt \le \dot{s}_\gamma^{\max}, \tag{8e}$$
$$\ddot{c}_\gamma^{\min} \le (\dot{c}_{\gamma(t_e+dt)} - \dot{c}^e_{\gamma(t_e)})/dt \le \ddot{c}_\gamma^{\max}. \tag{8f}$$
$$-\mu \le \ddot{c}_{\gamma(t_e+dt)}/g \le \mu, \tag{8g}$$

where $s_{\gamma(k)}$ and $s_{\gamma(k-1)}$ separately denote the step length and width generated by the current and the last optimization loop, $\dot{c}_{\gamma(t_e+dt)}$ and $\dot{c}^e_{\gamma(t_e)}$ separately denote the generated CoM velocity for the next sampling time and estimated CoM velocity at the current time moment, $\ddot{c}_{\gamma(t_e+dt)}$ is the generated CoM acceleration for the next sampling time.

Eq. (8a)$\sim$(8c) restrict the variation of the current step time, by limiting t_{ch} and t_{sh}. In Eq. (8a) and Eq. (8b), we have

$$\delta T^{\min} = \max\{0, T^{\min} - t_e\}, \quad \delta T^{\max} = T^{\max} - t_e, \tag{9}$$

where $T^{\min}$ and $T^{\max}$ separately denote the minimal and the maximal step time. $\max(\cdot)$ represents the function to choose the maximal value among inputs.

Using Eq. (8d), the step length and step width are both restricted to satisfy the kinematic reachability, by assuming a rectangular reachable zone.

In Eqs. (8e) and (8f), the swing leg velocity and the change of CoM velocity are limited to obey the actuation capability.

Finally, the friction cone is obeyed to avoid slippage by imposing Eq. (8g), with μ being the friction coefficient.

C. QCQP solution

Section III-B establishes a constrained optimization problem. Particularly, the quadratic equality constraint in Eq. (8c) results in a nonconvex QCQP, which is expressed as

$$\begin{aligned} \underset{{}_1\boldsymbol{\mathcal{X}}}{\text{argmin}} \quad & \frac{1}{2}({}_1\boldsymbol{\mathcal{X}}^{\mathrm{T}})\mathbf{G}({}_1\boldsymbol{\mathcal{X}}) + \mathbf{g}^{\mathrm{T}}({}_1\boldsymbol{\mathcal{X}}), \\ \text{s.t.} \quad & \frac{1}{2}({}_1\boldsymbol{\mathcal{X}}^{\mathrm{T}})\mathbf{V}_j({}_1\boldsymbol{\mathcal{X}}) + \mathbf{v}_j^{\mathrm{T}}({}_1\boldsymbol{\mathcal{X}}) \le \sigma_j, \end{aligned} \tag{10}$$

where $\mathbf{G}$, $\mathbf{V}_j \in \mathbb{R}^{4\times4}$, $\mathbf{g}$, $\mathbf{v}_j \in \mathbb{R}^4$, and $\sigma_j \in \mathbb{R}$ specify the objective function and constraints with $j \in \{1, ..., 13\}$.

In [1], SQP was utilized to solve the non-convex problem. However, it could neither provide a reliable solution nor guarantee global convergence, which is undesired for closed-loop control. To tackle this issue, the SDR [27] is used to transform the QCQP as a convex semidefinite programming (SDP) problem, which is thus solved with global convergence. Using the off-the-shelf solver, such as *Mosek* [28], the SDP can be solved within 25ms[2], meeting real-time requirements.

Remark 1: The usage of SDR enables us to solve the relaxed optimization problem efficiently with global convergence. However, it is hard to guarantee that the global optimum of the relaxed problem is also that of the original QCQP in Eq. (10). In theory, the feasibility can be easily checked [27], and a decent solution of Eq. (10) could be obtained. A detailed analysis of the numerical performance will be discussed in Section V-A.

[2]The time cost is estimated on the embedded board on Walker2 robot (Linux 14.04 with Intel i5 1.6 GHz CPU).

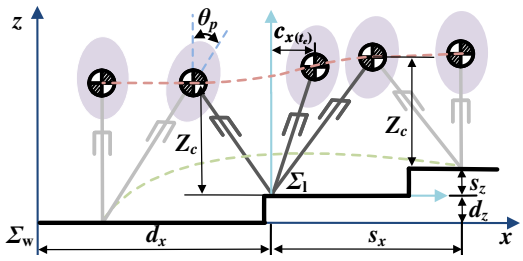

Fig. 4. NIPF moves in the sagittal plane. The red dashed curves plot the CoM trajectory. d_z is the vertical (global) step location.

IV. Angular Momentum Regulation via MPC

This section details LMPC for angular momentum modulation. Using the reduced-order NIPF model, angular momentum is regulated via upper-body rotation, which helps to manipulate the CMP movement [24]. Furthermore, to enhance adaptability, height variation in 3D walking is explicitly considered.

A. NIPF dynamics: body rotation with height variation

Assuming a flywheel at the CoM, the change of angular momentum is characterized by the upper-body rotation. To account for the height variation, the NIPF model [9] is used here, as plotted by Fig. 4. Then, the CMP is determined by

$$\begin{aligned} cmp_x &= \underbrace{c_x - \ddot{c}_x/\omega^2}_{p_x^h} - \dot{L}_y^g/(m(g+\ddot{c}_z)), \\ cmp_y &= \underbrace{c_y - \ddot{c}_y/\omega^2}_{p_y^h} + \dot{L}_x^g/(m(g+\ddot{c}_z)), \end{aligned} \tag{11}$$

where $w = \sqrt{(g+\ddot{c}_z)/(c_z - d_z)}$ is the time-varying natural frequency. $[\dot{L}_x^g, \dot{L}_y^g]^{\mathrm{T}}$ denote the change rate of angular momentum, which is given by

$$\dot{L}_x^g \approx I_{xx}^g \ddot{\theta}_r, \quad \dot{L}_y^g \approx I_{yy}^g \ddot{\theta}_p. \tag{12}$$

In Eq. (12), $[I_{xx}^g, I_{yy}^g]^{\mathrm{T}}$ are the first two diagonal components of the global angular momentum matrix $\mathbf{I}^g$. Assuming that the body inclination does not vary a lot over the prediction horizon, $\mathbf{I}^g$ is then determined by

$$\mathbf{I}^g = \mathbf{R}(\boldsymbol{\theta}^e)^{\mathrm{T}} \mathbf{I}_B \mathbf{R}(\boldsymbol{\theta}^e), \tag{13}$$

where $\mathbf{I}_B \in \mathbb{R}^{3\times3}$ is the inertia tensor in body coordinate, $\boldsymbol{\theta}^e \in \mathbb{R}^3$ denotes the estimated inclination angle. $\mathbf{R}(\boldsymbol{\theta}^e) \in \mathbb{R}^{3\times3}$ is the rotation matrix.

1) Prediction model: Choosing the current state $\hat{\boldsymbol{x}}_{(k)} = [x_{(k)}, \dot{x}_{(k)}]^{\mathrm{T}}$ ($x \in \{\theta_r, \theta_p\}$), we can predict the next state as

$$\hat{\boldsymbol{x}}_{(k+1)} = \underbrace{\begin{bmatrix} 1 & {}_2dt \\ 0 & 1 \end{bmatrix}}_{\mathbf{A}} \hat{\boldsymbol{x}}_{(k)} + \underbrace{\begin{bmatrix} ({}_2dt)^2 \\ {}_2dt \end{bmatrix}}_{\mathbf{B}} \ddot{x}_{(k)}, \tag{14}$$

where $\mathbf{A} \in \mathbb{R}^{2\times2}$ and $\mathbf{B} \in \mathbb{R}^2$ are both time-invarying that are determined in advance by ${}_2dt$.

Then, following Eq. (11), the output CMP at the j-th step ($j \in \{1, \ldots, N_h\}$) in the prediction window are

$$\begin{bmatrix} cmp_{x(k+j)} \\ cmp_{y(k+j)} \end{bmatrix} = \underbrace{\begin{bmatrix} p^h_{x(k+j)} \\ p^h_{y(k+j)} \end{bmatrix}}_{\mathbf{C}} + \underbrace{\begin{bmatrix} 0, & -\frac{I^g_{yy}}{m(g+\ddot{c}_{z(k+j)})} \\ \frac{I^g_{xx}}{m(g+\ddot{c}_{z(k+j)})}, & 0 \end{bmatrix}}_{\mathbf{D}} \ddot{\boldsymbol{\theta}}_{(k+j)}, \tag{15}$$

where $\ddot{\boldsymbol{\theta}}_{(k+j)} = [\ddot{\theta}_{r(k+j)}, \ddot{\theta}_{p(k+j)}]^{\mathrm{T}}$ consists of roll and pitch accelerations at the j-th step. $[p^h_{x(k+j)}, p^h_{y(k+j)}]^{\mathrm{T}}$ are the CoP.

Assuming a constant pendulum height (Z_c) at the beginning and the end of each step (see Fig. 4), the height trajectory can be obtained by the 5-th order polynomial interpolation, considering the continuity of position, velocity and acceleration. If the resultant CoP, i.e., $[p^h_x, p^h_y]$ computed by Eq. (11), goes beyond the support region, we use linear interpolation to generate the vertical height. In this way, CoP stays within the support region. And, $\mathbf{C} \in \mathbb{R}^{2\times 1}$ and $\mathbf{D} \in \mathbb{R}^{2\times 2}$ in Eq. (15) are determined in advance.

Using Eqs. (14) and (15), the rotation and CMP state over the horizon prediction can be obtained, given the future control inputs $\ddot{\boldsymbol{\theta}}_{(k+j)}$ [29]. We omit the details here for brevity.

B. MPC formulation

1) Cost function: We manipulate the CMP motion during the walking process by penalizing the deviation of body rotation angles. We also minimize the angular accelerations, i.e., control inputs, to achieve smooth movements. That is,

$$\begin{aligned} {}_2f({}_2\boldsymbol{\mathcal{X}}) = &\sum_{{}_2\boldsymbol{X}} \left\{ \frac{\alpha_{{}_2\boldsymbol{X}}}{2} \| {}_2\boldsymbol{X}_{(k)} - {}_2\boldsymbol{X}^r_{(k)} \|^2 + \frac{\beta_{{}_2\boldsymbol{X}}}{2} \| {}_2\ddot{\boldsymbol{X}}_{(k)} \|^2 \right\} \\ &+ \sum_{\boldsymbol{cmp}} \frac{\gamma_{\boldsymbol{cmp}}}{2} \| \boldsymbol{cmp}_{(k)} - \boldsymbol{cmp}^r_{(k)} \|^2, \end{aligned} \tag{16}$$

where ${}_2\boldsymbol{X}_{(k)} \in \{\boldsymbol{\theta}_{r(k)}, \boldsymbol{\theta}_{p(k)}\}$ and ${}_2\ddot{\boldsymbol{X}}_{(k)} \in \{\ddot{\boldsymbol{\theta}}_{r(k)}, \ddot{\boldsymbol{\theta}}_{p(k)}\}$ separately comprise the roll and pitch angles and angular accelerations over the prediction horizon, e.g, $\boldsymbol{\theta}_{r(k)} = [\theta_{r(k+1)}, \ldots, \theta_{r(k+N_h)}]^{\mathrm{T}}$, $\boldsymbol{cmp} \in \{\mathbf{cmp}_x, \mathbf{cmp}_y\}$ denotes the predicted CMP, $\alpha_{{}_2\boldsymbol{X}}$, $\beta_{{}_2\boldsymbol{X}}$ and $\gamma_{\boldsymbol{cmp}}$ are weights.

Control inputs (${}_2\boldsymbol{\mathcal{X}} \in \mathbb{R}^{2\times N_h}$) are the angular acceleration over the prediction horizon, namely, ${}_2\boldsymbol{\mathcal{X}} = [\ddot{\boldsymbol{\theta}}_{r(k)}; \ddot{\boldsymbol{\theta}}_{p(k)}]$. By default, the reference body rotation angles ${}_2\boldsymbol{X}^r_{(k)}$ are zeros. And, the reference CMP positions ($\boldsymbol{cmp}^r_{(k)}$) coincide with the support center, i.e., the step location, which is already generated by the first-layer QCQP.

2) Feasibility constraints: The trunk rotation is restricted to comply with the articulation limit and actuation capability. Taking the roll angle as an example, we have linear constraints

$$\begin{aligned} &\theta^{\min}_r \le \theta_{r(k+i)} \le \theta^{\max}_r, \\ &\tau^{\min}_r \le I_x \ddot{\theta}_{r(k+i)} \le \tau^{\max}_r, \quad i \in \{1, ..., N_h\}, \end{aligned} \tag{17}$$

where $\{\theta^{\min}_r, \theta^{\max}_r\}$ and $\{\tau^{\min}_r, \tau^{\max}_r\}$ are the lower and upper boundaries of roll angle and torque, respectively.

Note that the CMP can go beyond the support region without resulting in a fall [24]. Thus, we do not restrict the CMP motion within the support region, which is different from the LMPC structure in [23], [30].

TABLE II
PARAMETER SETTINGS FOR WALKER2 GAIT OPTIMIZATION

1. Default parameters			
s^r_x/s^r_y[m]	0.1/0.22	T^r[s]	0.7
s^r_z[m]	0	Z_c[m]	0.5
dt[s]	0.025	${}_2dt$[s]	0.01
2. Constraint boundaries for QCQP			
$s^{\min}_x/s^{\max}_x$[m]	-0.15/0.3	$T^{\min}/T^{\max}$[s]	0.5/1.2
$s^{\min}_y/s^{\max}_y$[m]	0.12/0.25	μ	0.75
$\dot{s}^{\min}_x/\dot{s}^{\max}_x$[m·s^{-1}]	-2.5/3	$\dot{c}^{\min}_x/\dot{c}^{\max}_x$[m·s^{-2}]	-5/5
$\dot{s}^{\min}_y/\dot{s}^{\max}_y$[m·s^{-1}]	-1/2	$\dot{c}^{\min}_y/\dot{c}^{\min}_y$[m·s^{-2}]	-6/6
3. Constraint boundaries for LMPC			
$\theta^{\min}_r/\theta^{\max}_r$[rad]	-0.17/0.17	$\tau^{\min}_r/\tau^{\max}_r$[N·m]	-20/20
$\theta^{\min}_p/\theta^{\max}_p$[rad]	-0.17/0.17	$\tau^{\min}_p/\tau^{\max}_p$[N·m]	-20/20

The above LMPC is formulated as a convex QP, which is expressed as

$$\begin{aligned} \underset{{}_2\boldsymbol{\mathcal{X}}}{\operatorname{argmin}} \quad & \frac{1}{2}({}_2\boldsymbol{\mathcal{X}}^{\mathrm{T}})\mathbf{H}({}_2\boldsymbol{\mathcal{X}}) + \mathbf{h}^{\mathrm{T}}({}_2\boldsymbol{\mathcal{X}}), \\ \text{s.t.} \quad & \mathbf{q}^{\mathrm{T}}_j({}_2\boldsymbol{\mathcal{X}}) \le q_j, \quad j \in \{1, ..., N_c\}, \end{aligned} \tag{18}$$

where $\mathbf{H} \in \mathbb{R}^{N_t \times N_t}$, $\mathbf{h}$, $\mathbf{q}_j \in \mathbb{R}^{N_t}$, and $q_j \in \mathbb{R}$ specify the objective function and constraints, N_t and N_c are the number of decision variables and constraints. Here, we have $N_t = 2N_h$ and $N_c = 8N_h$ with N_h being the prediction length.

In this work, we use 'OSQP' [31] to solve the above problem. For the MPC, the prediction horizon for LMPC is 0.1s and the prediction length N_h is 10. It turns out that the LMPC can be solved within 10ms using the onboard computer.

As a result, by using the above sequential optimization method, the stepping and hip strategy are integrated. Particularly, following the NIPF dynamics, our formulation is applicable to 3D locomotion with variable height, which can not be realized by the work in [11], [12], [17] and [18].

V. EVALUATIONS

We validate the proposed method in this section. Particularly, COMAN robot (pelvis height: 0.465m, weight: 31kg) [32] is employed in simulation and the Walker2 robot (pelvis height: 0.5m, weight: 70kg) [33] is utilized for hardware tests. For COMAN robot, the default step width is 0.1452m. For Walker2 robot, the default step time is 0.7s. Furthermore, for Walker2 robot, we assume the CoM is located above the pelvis center with a 0.1m offset. Some other parameters for Walker2 gait optimization are listed in Table II. For both robots, the double support phase takes 20% of one stepping cycle. The results can be addressed at https://youtu.be/YeK8jWwRbyo.

A. Template evaluation

1) Push recovery with stepping strategy: Push recovery with the stepping strategy is demonstrated by the LIP simulation using the physical property of the COMAN robot. The default T is 0.8s, and the default s_x is 0.1m. During the walking process, the horizontal push forces (lasting 0.1s) were imposed at the pelvis center. Specifically, the backward

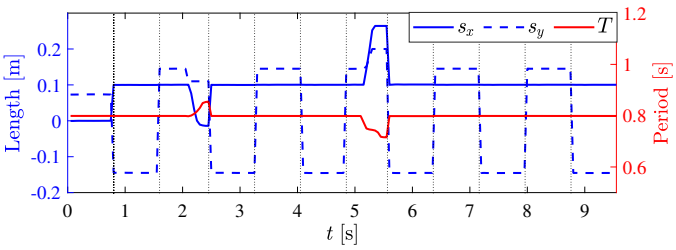

Fig. 5. Evolutionary step parameters for push recovery. Dotted lines mark the switch between different step cycles.

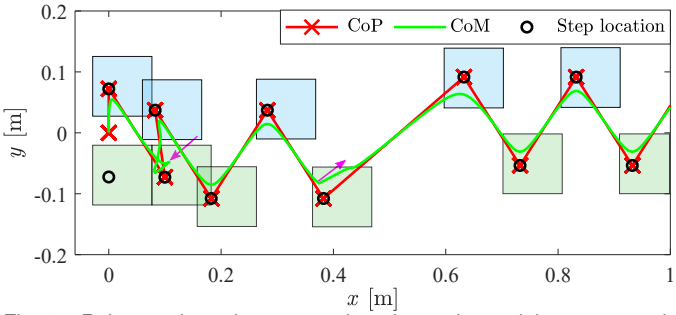

Fig. 6. Robust gait against external pushes, where pink arrows mark the push forces. Green and blue blocks separately mark the right and left step locations.

200N and rightward 100N force was imposed at 2s, while the forward 300N and leftward 150N force was imposed at 5s.

As illustrated in Fig. 5, the robot rejected external pushes by adjusting step parameters timely. For example, at 2s with the right support, the robot landed on the ground later with a shorter step length and width since the external force pulled the robot right behind, as shown in Fig. 5. Numerical analysis reveals that the step time (T) extended to 0.816s, and the step length (s_x) and width (s_y) separately dropped to -0.017m and 0.11m. Using the updated step parameters, the CoM trajectory was generated, see the green curve in Fig. 6. Notably, the generated CoP is always located at the support center. Thus, the locomotion stability is guaranteed.

2) Comparison study: To further validate the advantages of this work, we compare it with our previous work [1] where SQP was used to solve the NLP problem. Then, we compare our stepping strategy with [18] and [17]. In [18], a QP was formulated to adjust the step parameters by manipulating the divergent component of motion (DCM) offset. In [17], a QP was first employed to adjust the step time, and an MPC was then solved for step location, considering the CoP movement within the support region.

1, Robustness: We first compare the maximum push pulse each approach can reject along various directions. In each test, a constant horizontal force lasting 0.1s was applied to the trunk at the middle of a step when the right foot touched the ground. In each scenario, each method runs four times with different weights, and the average values are reported in Fig. 7.

The green curve in Fig. 7 demonstrates that the maximum push pulse our approach can reject varies a lot as the push direction changes. Particularly, due to the collision limit, the robot rejects much less external push along $240^\circ \sim 330^\circ$ than other directions. Nevertheless, the SDR results in a much

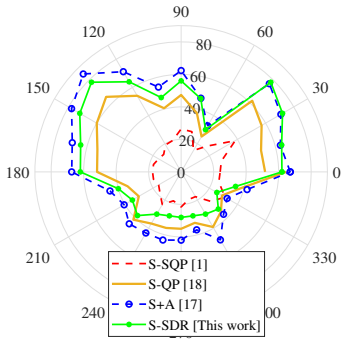

Fig. 7. Comparison of the maximal push impulse (in N·s) the robot can recover from when using different approaches. $\theta = 0^\circ$ and $\theta = 90^\circ$ represent the forward and left directions, respectively. 'S' and 'A' separately denote the stepping and ankle strategy.

TABLE III
TIME COSTS NEEDED BY DIFFERENT APPROACHES

Strategy	S [1]	S [18]	S+A [17]	S [This work]
Solver	SQP	QP	QP+QP	SDR
Time cost [s]	0.7±0.2	0.3±0.1	8±1.5	3.8±0.9

higher push recovery capability than the previous work in [1] in almost all directions (except along 330°). On average, the maximal pulse it can reject increases by 135%. The DCM-based work in [18] can reject larger external pushes along $225^\circ \sim 345^\circ$. That is because the DCM offset is allowed in the lateral direction, working implicitly as an ankle strategy.

Note that the work in [17] rejects the largest external push from most directions due to the integration of the ankle and stepping strategy (denoted by 'S+A'). However, in specific directions, such as $15^\circ \sim 45^\circ$, [17] does not perform the best. We guess it is because [17] optimizes the step time and location in a strict order, limiting its search space. Aside from this, our work assumes no CoP motion, enabling the application to robots with point or linear feet.

2, Computing efficiency: Table III summarizes the time costs (1000 trials) needed by different approaches[3], with the i7 2.1 GHz quad-core CPU. We found that the stepping strategy in [18] is the most efficient since only a small QP is solved. When solving the QCQP using SDR, this work leads to a larger time cost than [1]. However, it is still fast enough.

B. Robust walking on real flat surface

In this section, we present experimental results on push recovery when engaging different balance strategies.

1) recovery from ball strikes with/without stepping strategy engaged: As can be seen from the first column in Fig. 8, a 6kg ball attached to a rope was released from a fixed height (the rope length is 1m and the release angle $\mathbf{\Phi}$ is 30°) when the robot was stepping in place. Then, the ball hit the robot repeatedly until the kinetic energy was totally dissipated.

With stepping strategy engaged, the robot adjusted step parameters, including step time T and step width s_y (see Table IV), while adjusting CoM motion (see 'c_x' and 'c_y' in Fig. 9(a) and (b)) to maintain balance. Particularly, when

[3]Considering the second-layer LMPC in our work can be solved fast by a small-scale QP, we do not report the time cost here.

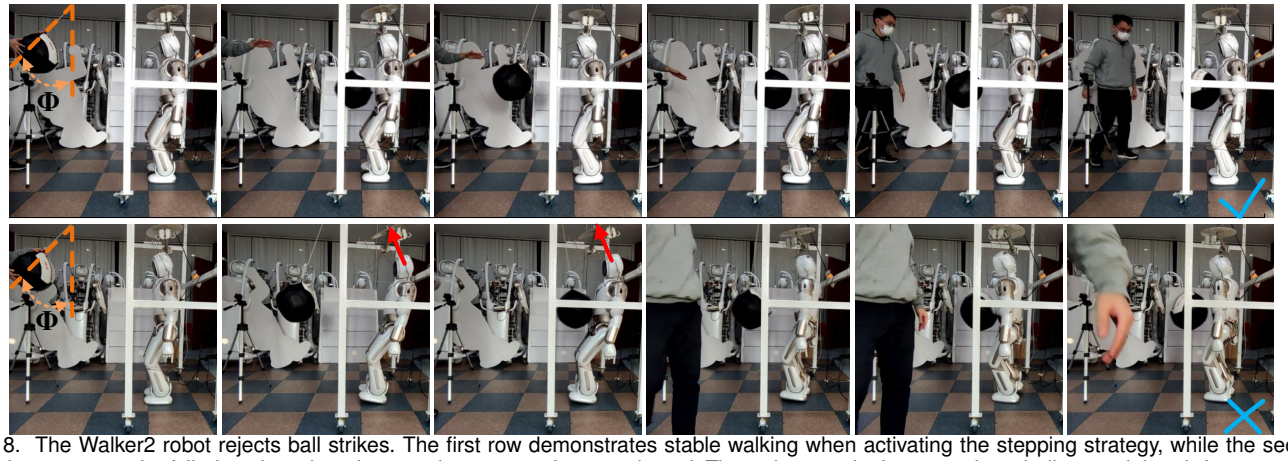

Fig. 8. The Walker2 robot rejects ball strikes. The first row demonstrates stable walking when activating the stepping strategy, while the second row demonstrates the failed motion when the stepping strategy is not activated. The red arrows in the second row indicate a tight rob for protection.

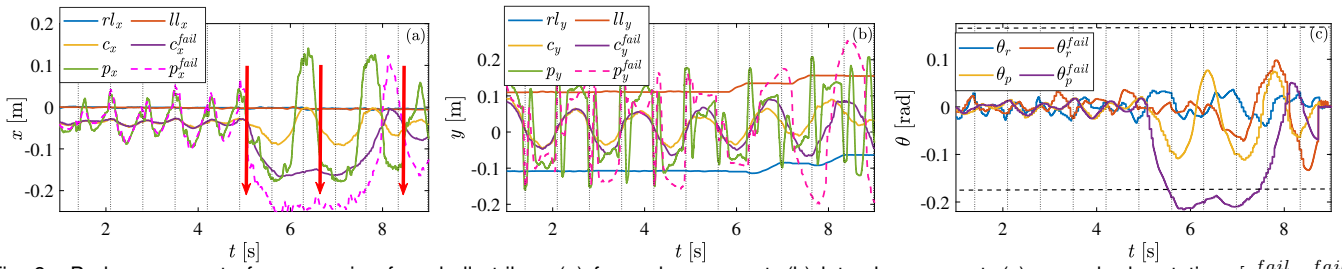

Fig. 9. Body movements for recovering from ball strikes: (a) forward movement, (b) lateral movement, (c) upper-body rotation. $[c_x^{fail}, c_y^{fail}]$, $[p_x^{fail}, p_y^{fail}]$ and $[\theta_r^{fail}, \theta_p^{fail}]$ separately denote the horizontal CoM trajectory, CoP trajectory and body rotation angles when no stepping strategy was used. $[rl_x, rl_y]$ and $[ll_x, ll_y]$ separately denote the right and left leg trajectory along x- and y- axis. Red arrows in (a) mark the time moments when the ball strikes the robot body. Dashed lines in (c) mark the upper and lower boundaries of body rotations.

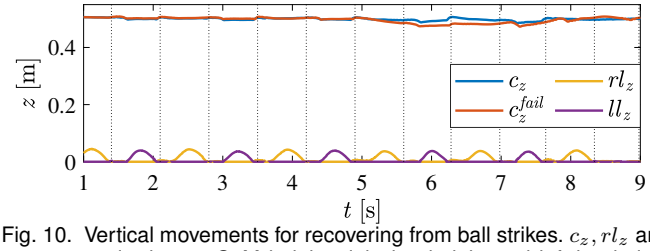

Fig. 10. Vertical movements for recovering from ball strikes. c_z, rl_z and ll_z separately denote CoM height, right leg height and left leg height when the stepping strategy was used. c_z^{fail} plots the CoM height when the stepping strategy was not activated.

TABLE IV
STEP PARAMETERS MODULATION FOR REJECTING BALL STRIKES

Parameter \ step	9	10	11	12	13	others
s_x [m]	-0.001	0.001	0	0	0	0
$\|s_y\|$ [m]	0.25	0.22	0.25	0.22	0.25	0.22
T [s]	0.68	0.7	0.68	0.7	0.64	0.7

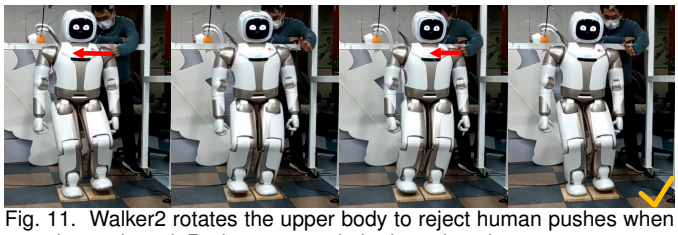

Fig. 11. Walker2 rotates the upper body to reject human pushes when stepping on board. Red arrows mark the lateral pushes.

the ball strike happened, the robot adopted a smaller step time (e.g., T changed from 0.7s to 0.68s at the 9-th step), meaning a higher stepping frequency. Meanwhile, the robot modulated the upper-body rotation angles (see 'θ_p' in Fig. 9(c)). Using the LMPC, the rotation angle fell in the feasible region.

Correspondingly, using the updated step parameters, adaptive leg trajectories were synthesized, as plotted by Fig. 9 and 10. The c_z plot in Fig. 10 demonstrates that, when the ball stopped moving (after about 7.5s), the robot returned to the nominal gait with a constant height.

On the contrary, when the stepping strategy was not activated, which could be realized by setting large weights (i.e., σ_{1x} in Eq. (6)), the robot tipped over. Corresponding plots in Fig. 9 demonstrate larger oscillations in forward trajectories, including c_x^{fail}, p_x^{fail} and θ_p^{fail}, from 3s to 6s. Also, undesired p_y^{fail} and θ_r^{fail} are observed.

2) recovery from human pushes with/without hip strategy: Due to the hierarchical structure, the second-layer hip strategy can be engaged alone to reject external disturbances when step variation is restricted. To demonstrate this, we pushed the robot when it stepped on the board, see Fig. 11. In this case, the stepping strategy was not engaged. When the second-layer hip strategy was engaged, the robot maintained balance when encountering multiple lateral pushes, as can be seen in Fig. 11. In contrast, when the hip strategy was not activated, the robot fell, which can be found in the attached video.

3) push recovery when walking forward: Push recovery when walking forward is also tested. In this case, the default T is 0.7s, and the default s_x is 0.1m. Using the proposed stepping and hip strategies, the robot rotated the upper body and

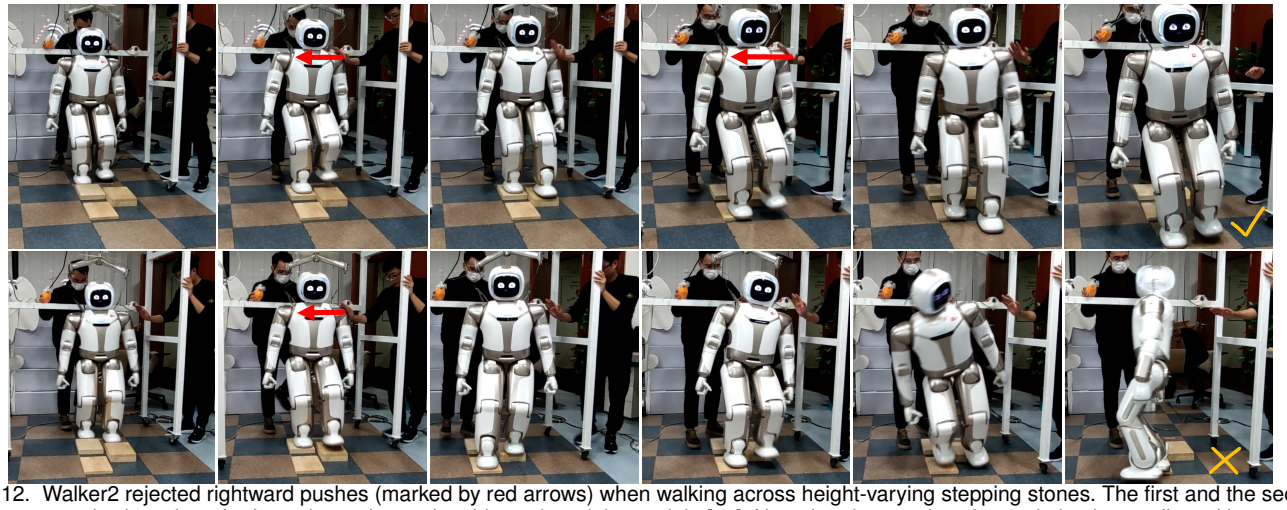

Fig. 12. Walker2 rejected rightward pushes (marked by red arrows) when walking across height-varying stepping stones. The first and the second rows separately show the robot's motions when using this work and the work in [23]. Note that the step location variation is not allowed here.

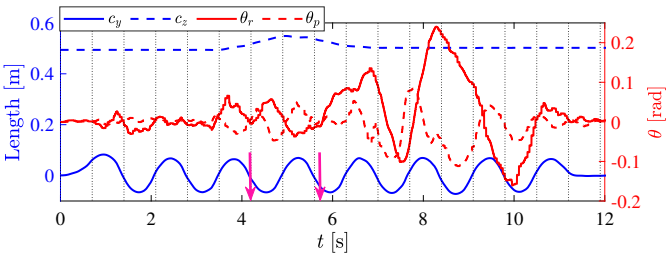

Fig. 13. Body movement for the Walker2 robot when walking across stepping stones with variable height. Pink arrows mark the time moments when external pushes were imposed.

adjusted step parameters to maintain balance when external pushes were imposed. Please check the video for more details.

C. Robust walking across height-varying stepping stones

A more challenging scenario where human pushes were applied when the robot stepped across stepping stones at various heights is considered. The heights of stepping stones are 3cm, 4cm and 1cm, respectively. To accommodate for the uneven terrain, a time-varying CoM height trajectory was generated in advance. In this case, the variation of step location is forbidden.

Fig. 12 shows that with the proposed controller, the robot successfully walked across the sparse steppable region when encountering rightward push forces, by modulating the inclination status of the upper body (plotted by the red solid curve ('θ_r') in Fig. 13). Also, the step time slightly changed. For example, the step period of the seventh step changed from 0.7s to 0.69s. In contrast, using [23], the robot would fall. Please check the video for more details. The reason is that the work in [23] does not modulate step time. Also, the CMP is strictly constrained there, limiting the body rotation.

Notably, in our test, we did not slow down the step frequency, meaning that the robot passed across the uneven ground at the normal speed. To our knowledge, push recovery in this challenging scenario has never been discussed by most of the existing work that could activate stepping strategies or multiple strategies, such as [11], [17], [18]. It is interesting that

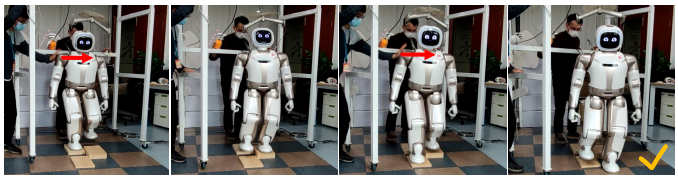

Fig. 14. Walker2 rejected multiple leftward pushes (marked by red arrows) when walking across the uneven ground.

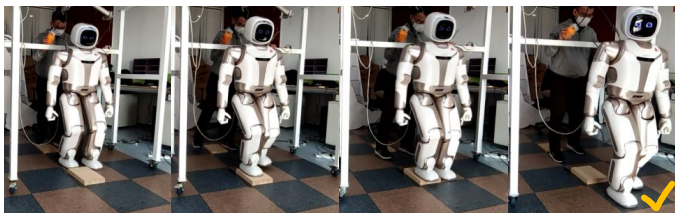

Fig. 15. Walker2 robot walks across a stepping stone.

push recovery when walking across uneven ground is analyzed in [10] and [21]. But to our best knowledge, no hardware validation is provided by [10]. In [21], only one single push was imposed on the body when the robot was walking across the uneven ground. Besides, in [21], the steppable region is set large enough to allow the modulation of step locations, resulting in an easier task than ours.

Besides, walker2 could also reject leftward pushes when walking across sparse stepping stones, as illustrated in Fig. 14. For more details, please check the attached video.

D. 3D versatile walking: ablation studies

In addition to robust locomotion, we also demonstrate that the Walker2 robot could accomplish 3D versatile tasks using only the second-layer LMPC scheme. One example is that the robot walked across a stepping stone (4cm in height). In this case, the robot maintained balance by modulating the upper-body status while explicitly considering the height variation as well. The hardware motion is illustrated in Fig. 15. Also, the robot could walk stably with time-varying step parameters, as can be seen in the attached video.

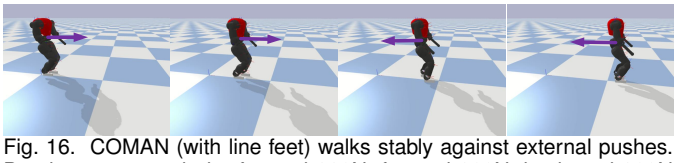

Fig. 16. COMAN (with line feet) walks stably against external pushes. Purple arrows mark the forward 320N, forward 300N, backward 300N and backward 300N pushes, respectively. Each push lasts 0.1s.

E. Stable walking of a humanoid robot with line feet

As mentioned in Section III, since we assume no CoP movement during each step, no finite foot size is required. As a result, the proposed approach can be applied to humanoid robots with line or point feet. Taking the COMAN robot with line feet (length: 15cm, width: 2cm) as an example, we validate the robust locomotion via dynamic simulations in *PyBullet*. Simulations were run at 200Hz, and the nominal T was 0.5s. Fig. 16 visualizes the robust locomotion against sagittal pushes when stepping forward (the default s_x is 0.1m). As can be seen from Fig. 16 and the attached video, due to the smaller contact zone, the robot slid on the surface and rotated along the z-axis when external forces were imposed. Nevertheless, the balance was maintained using the proposed method.

Aside from this, COMAN could realize stable walking with variable step parameters, as can be seen from the video.

VI. Conclusions and Discussions

In this work, robust locomotion in real-world scenarios is accomplished via sequential convex optimization. First, optimal step parameters (i.e., step time and location) under external disturbances are obtained in real-time by solving a QCQP problem. Then, upper-body rotation is adjusted by a fast linear MPC. By explicitly characterizing vertical motion, adaptable locomotion in 3D scenarios with height variation is also accomplished. The comparison with state-of-the-art validates the enhanced robustness and adaptability of the proposed method. Extensive evaluations with the full-sized COMAN and Walker2 robots demonstrate the effectiveness in achieving challenging locomotion tasks, such as rejecting pushes when walking across stepping stones with height variation.

Nevertheless, there is still room for improvement. First, we acknowledge that using SDR in Section III-C enables us to solve the relaxed problem efficiently with global convergence. However, it is hard to guarantee that the global optimum of the relaxed problem is also that of the original QCQP in Section III-B. To make a tight relaxation, we can take the SDR solution as an initial guess and feed it to a general nonlinear optimization solver, such as SQP. Furthermore, in future work, we can integrate the ankle strategy in the future to enhance robustness, following the idea in [11], [25]. Aside from these, the current low-level tracking controller ignores the mass distribution in limbs, weakening the locomotion performance. We are keen to apply a whole-body tracking controller [34], [35] in future.

Acknowledgments

This work is supported by the EU project 101016970 NI and the EU Horizon 2020 research and innovation programme under the Marie Skłodowska-Curie grant agreement No 101018395. Also, the work is supported in part by the Program of Guangdong Provincial Key Laboratory of Robot Localization and Navigation Technology, under grant 2020B121202011.

References

[1] J. Ding, X. Xiao, and N. G. Tsagarakis, "Nonlinear optimization of step duration and step location," in *Proc. IEEE/RSJ Int. Conf. Intell. Robot. Syst.*, 2019, pp. 2849–2854.

[2] R. C. Luo and C. C. Chen, "Biped walking trajectory generator based on three-mass with angular momentum model using model predictive control," *IEEE Trans. Ind. Electron.*, vol. 63, no. 1, pp. 268–276, 2015.

[3] D. Ahn and B. Cho, "Online jumping motion generation via model predictive control," *IEEE Trans. Ind. Electron.*, vol. 69, no. 5, pp. 1706–1715, May 2022.

[4] D. Yao, L. Yang, X. Xiao, and M. Zhou, "Velocity-based gait planning for underactuated bipedal robot on uneven and compliant terrain," *IEEE Trans. Ind. Electron.*, vol. 69, no. 11, pp. 11 414–11 424, 2021.

[5] X. Xiong and A. Ames, "3-d underactuated bipedal walking via h-lip based gait synthesis and stepping stabilization," *IEEE Trans. Robot.*, vol. 38, no. 4, pp. 2405–2425, 2022.

[6] Z. He and K. Yamamoto, "Decoupling of inertia effect in angular momentum of a humanoid and its application to resolved viscoelasticity control," in *Proc. IEEE Int. Conf. Robot. Autom.*, 2022, pp. 8490–8496.

[7] K. Van Heerden, "Real-time variable center of mass height trajectory planning for humanoids robots," *IEEE Robot. Autom. Lett.*, vol. 2, no. 1, pp. 135–142, Jan. 2017.

[8] S. Kajita, F. Kanehiro, K. Kaneko, K. Yokoi, and H. Hirukawa, "The 3d linear inverted pendulum mode: A simple modeling for a biped walking pattern generation," in *Proc. IEEE/RSJ Int. Conf. Intell. Robot. Syst.*, vol. 1, 2001, pp. 239–246.

[9] S. Kajita, H. Hirukawa, K. Harada, and K. Yokoi, *Introduction to humanoid robotics*. Springer Berlin Heidelberg, 2014, vol. 101.

[10] K. Guan, K. Yamamoto, and Y. Nakamura, "Push recovery by angular momentum control during 3d bipedal walking based on virtual-mass-ellipsoid inverted pendulum model," in *Proc. IEEE-RAS Int. Conf. Humanoid Robots*, 2019, pp. 120–125.

[11] J. Choe, J.-H. Kim, S. Hong, J. Lee, and H.-W. Park, "Seamless reaction strategy for bipedal locomotion exploiting real-time nonlinear model predictive control," *IEEE Robot. Autom. Lett.*, pp. 1–8, 2023.

[12] H. Jeong, I. Lee, J. Oh, K. K. Lee, and J.-H. Oh, "A robust walking controller based on online optimization of ankle, hip, and stepping strategies," *IEEE Trans. Robot.*, vol. 35, no. 6, pp. 1367–1386, Dec. 2019.

[13] Z. Aftab, T. Robert, and P.-B. Wieber, "Ankle, hip and stepping strategies for humanoid balance recovery with a single model predictive control scheme," in *Proc. IEEE-RAS Int. Conf. Humanoid Robots*, 2012, pp. 159–164.

[14] P. Kryczka, P. Kormushev, N. G. Tsagarakis, and D. G. Caldwell, "Online regeneration of bipedal walking gait pattern optimizing footstep placement and timing," in *Proc. IEEE/RSJ Int. Conf. Intell. Robot. Syst.*, 2015, pp. 3352–3357.

[15] M. R. Maximo, C. H. Ribeiro, and R. J. Afonso, "Mixed-integer programming for automatic walking step duration," in *Proc. IEEE/RSJ Int. Conf. Intell. Robot. Syst.*, 2016, pp. 5399–5404.

[16] R. Zhang, L. Meng, Z. Yu, X. Chen, H. Liu, and Q. Huang, "Stride length and stepping duration adjustments based on center of mass stabilization control," *IEEE/ASME Trans. Mechatron.*, vol. 27, no. 6, pp. 5005–5015, 2022.

[17] F. M. Smaldone, N. Scianca, L. Lanari, and G. Oriolo, "Feasibility-driven step timing adaptation for robust mpc-based gait generation in humanoids," *IEEE Robot. Autom. Lett.*, vol. 6, no. 2, pp. 1582–1589, 2021.

[18] M. Khadiv, A. Herzog, S. A. A. Moosavian, and L. Righetti, "Walking control based on step timing adaptation," *IEEE Trans. Robot.*, vol. 36, no. 3, pp. 629–643, June 2020.

[19] F. Nazemi, A. Yousefi-Koma, M. Khadiv *et al.*, "A reactive and efficient walking pattern generator for robust bipedal locomotion," in *Prof. 5th RSI Int. Conf. Robot. Mechatron.*, 2017, pp. 364–369.

[20] Y. Kojio, Y. Omori, K. Kojima, F. Sugai, Y. Kakiuchi, K. Okada, and M. Inaba, "Footstep modification including step time and angular momentum under disturbances on sparse footholds," *IEEE Robot. Autom. Lett.*, vol. 5, no. 3, pp. 4907–4914, July 2020.

[21] S. Sato, Y. Kojio, Y. Kakiuchi, K. Kojima, K. Okada, and M. Inaba, "Robust humanoid walking system considering recognized terrain and robots' balance," in *Proc. IEEE/RSJ Int. Conf. Intell. Robot. Syst.*, 2022, pp. 8298–8305.
[22] S. Caron, A. Escande, L. Lanari, and B. Mallein, "Capturability-based pattern generation for walking with variable height," *IEEE Trans. Robot.*, vol. 36, no. 2, pp. 517–536, 2019.
[23] J. Ding, L. Han, L. Ge, Y. Liu, and J. Pang, "Robust locomotion exploiting multiple balance strategies: An observer-based cascaded model predictive control approach," *IEEE/ASME Trans. Mechatron.*, vol. 27, no. 4, pp. 2089–2097, August, 2022.
[24] M. B. Popovic, A. Goswami, and H. Herr, "Ground reference points in legged locomotion: Definitions, biological trajectories and control implications," *Int. J. Robot. Res.*, vol. 24, no. 12, pp. 1013–1032, Dec. 2005.
[25] J. Ding, X. Xiao, N. G. Tsagarakis, and Y. Huang, "Robust gait synthesis combining constrained optimization and imitation learning," in *Proc. IEEE/RSJ Int. Conf. Intell. Robot. Syst.*, 2020, pp. 3473–3480.
[26] S. Kajita, M. Morisawa, K. Miura, S. Nakaoka, K. Harada, K. Kaneko, F. Kanehiro, and K. Yokoi, "Biped walking stabilization based on linear inverted pendulum tracking," in *Proc. IEEE/RSJ Int. Conf. Intell. Robot. Syst.*, 2010, pp. 4489–4496.
[27] Z.-Q. Luo, W.-K. Ma, A. M.-C. So, Y. Ye, and S. Zhang, "Semidefinite relaxation of quadratic optimization problems," *IEEE Signal Process. Mag.*, vol. 27, no. 3, pp. 20–34, May 2010.
[28] M. ApS, "Mosek fusion api for c++. version 9.0.86., 2019: https://www.mosek.com/downloads/9.0.86/."
[29] P.-B. Wieber, "Trajectory free linear model predictive control for stable walking in the presence of strong perturbations," in *Proc. IEEE-RAS Int. Conf. Humanoid Robots*, 2006, pp. 137–142.
[30] J. Lack, "Integrating the effects of angular momentum and changing center of mass height in bipedal locomotion planning," in *Proc. IEEE-RAS Int. Conf. Humanoid Robots*, 2015, pp. 651–656.
[31] B. Stellato, G. Banjac, P. Goulart, A. Bemporad, and S. Boyd, "Osqp: An operator splitting solver for quadratic programs," *Math. Program. Comput.*, vol. 12, no. 4, pp. 637–672, 2020.
[32] N. G. Tsagarakis, S. Morfey, G. M. Cerda, L. Zhibin, and D. G. Caldwell, "Compliant humanoid coman: Optimal joint stiffness tuning for modal frequency control," in *Proc. IEEE Int. Conf. Robot. Autom.*, 2013, pp. 673–678.
[33] *Ubtech Robotics Corporation: https://www.ubtrobot.com/cn/.*
[34] M. Neunert, M. Stäuble, M. Giftthaler, C. D. Bellicoso, J. Carius, C. Gehring, M. Hutter, and J. Buchli, "Whole-body nonlinear model predictive control through contacts for quadrupeds," *IEEE Robot. Autom. Lett.*, vol. 3, no. 3, pp. 1458–1465, 2018.
[35] D. Kim, J. Di Carlo, B. Katz, G. Bledt, and S. Kim, "Highly dynamic quadruped locomotion via whole-body impulse control and model predictive control," *arXiv preprint arXiv:1909.06586*, 2019.

Jiatao Ding received his B.Eng. Degree and Ph.D. Degree in Engineering from Wuhan University, China, in 2014 and 2020, respectively. From 2018-2020, he was a visiting Ph.D. student at the Italian Institute of Technology, Italy.

He is currently a Postdoctoral Researcher with the Department of Cognitive Robotics, Delft University of Technology, The Netherlands. His research interests include legged locomotion, robot learning and model predictive control.

Cosimo Della Santina received the Ph.D. degree in robotics from University of Pisa, Italy, in 2019. He was a Visiting Ph.D. student and a Postdoctoral Researcher (2017 to 2019) at Massachusetts Institute of Technology, USA. Since 2020, he has been affiliated with the German Aerospace Centre as an external research scientist.

He is currently an Assistant Professor with the Department of Cognitive Robotics, Delft University of Technology, The Netherlands. His research interests include modelling and Control of Soft Robots, robot learning on soft robotics and soft robotic hands.

Tin Lun Lam received his B.Eng. Degree and Ph.D. Degree in Robotics and Automation from the Chinese University of Hong Kong in 2006 and 2010, respectively.

He currently serves as Assistant Professor and Executive Deputy Director of the Robotics & AI Lab at the Chinese University of Hong Kong, Shenzhen and Director of the Research Center on Intelligent Robots of Shenzhen Institute of Artificial Intelligence and Robotics for Society. His research interests include field robotics, human-machine interaction, and intelligent control.

Jianxin Pang received his B.Eng. degree and Ph.D. degree from the University of Science and Technology of China in 2002 and 2008, respectively.

He is currently the director of UBTECH Research Institute. His interests include optimal control, machine learning, motion planning and their applications to humanoid robots, home service robots, and teaching robots.

Xiaohui Xiao received the B.S. and M.S. degrees in Mechanical Engineering from Wuhan University, Wuhan, China, in 1991 and 1998, respectively, and the Ph.D. degree in mechanical engineering from Huazhong University of Science and Technology, Wuhan, China, in 2005.

She is currently a Full Professor at the Department of Mechanical Engineering, Wuhan University. Her research interests are in the fields of humanoid bipedal robots, force control for cooperative robots, and high-precision positioning control.

Nikos G. Tsagarakis is currently a Tenured Senior Scientist with the Istituto Italiano di Tecnologia, Genoa, Italy, with overall responsibility for humanoid design and human centered mechatronics development. He has authored or co-authored over 250 papers in journals and at international conferences and holds 14 patents. He is currently a Senior Editor of the IEEE/ASME Transactions in Mechatronics.

Yanlong Huang received the Ph.D. degree from the Institute of Automation, Chinese Academy of Sciences, Beijing, China. He carried out his research as a Postdoctoral Researcher with the Max-Planck Institute for Intelligent Systems and Italian Institute of Technology. He is currently a University Academic Fellow with the School of Computing, University of Leeds, Leeds, U.K.

His interests include imitation learning, optimal control, and reinforcement learning. He is an Associate Editor for IEEE International Conference on Intelligent Robots and Systems (2022 - 2024), an Associate Editor for the IEEE Robotics and Automation Letters, and an Associate Editor for Transactions of the Institute of Measurement and Control.